JOURNAL OF COMPUTATIONAL PHYSICS 67, 372–395 (1986)

# On Nonlinear Instabilities in Leap-Frog Finite Difference Schemes

D. M. SLOAN

*Department of Mathematics, University of Strathclyde, Glasgow G1 1XH, Scotland*

AND

A. R. MITCHELL

*Department of Mathematical Sciences, The University, Dundee DD1 4HN, Scotland*

Received June 13, 1985; revised December 12, 1985

Briggs, Newell and Sarie (*J. Comput. Phys.* **51**, 83 (1983)) have discussed a mechanism for the destabilisation of finite difference approximations to nonlinear partial differential equations. Their ideas were developed using the leap-frog approximation to the advection equation. Here the same situation is examined in a manner which compares the basic solution to a periodic wavetrain. An investigation is made into the stability of the basic solution to small disturbances which take the form of side-band Fourier modes. The relation between side-band growth and envelope modulation is discussed. © 1986 Academic Press, Inc.

## 1. INTRODUCTION

A recent paper by Briggs, Newell and Sarie [3] described a focusing mechanism for the destabilisation of nonlinear partial difference equations. The authors correctly drew attention to the fact that little work has been done on analysing instabilities in nonlinear difference equations in the way that fluid dynamicists have analysed the instabilities associated with transition to turbulence. Briggs *et al.* confined their attention to leap-frog discretisations of the quasi-linear equation

$$u_t + uu_x = 0 \tag{1.1}$$

and they described a mechanism for the triggering of nonlinear instabilities. This mechanism is related to that which causes the disintegration of wavetrains on deep water, first suggested by Lighthill [7] and subsequently analysed in a classic paper by Benjamin and Feir [2]. The aim of this note is to supplement the interesting work of Briggs *et al.* by examining the same situation using methods related to those adopted by Benjamin and Feir [2]. It is important that appropriate com-



0021-9991/86 $3.00

parisons be made between instabilities in difference equations and instabilities in periodic wavetrains in fluids in order that maximum use might be made of the extensive literature in this latter area. The Benjamin and Feir approach has been used profitably to study instabilities in nonlinear, dispersive, differential systems by, inter alios, Yuen and Ferguson [12], Fornberg and Whitham [5] and Herbst, Mitchell and Weideman [6].

Suppose (1.1) has to be solved in the region $0 \leqslant x \leqslant 1$ and that the equation is discretised in space using a grid size $h = 1/J$, where $J$ is an even integer. Since the grid cannot resolve wavelengths smaller than $2h$ it follows that a Fourier mode $\exp(2\pi ijp/J)$, $j = 0, 1, \ldots, J$, satisfies the constraint $|p| \leqslant J/2$. If quadratic nonlinear interactions give rise to a mode $\exp(2\pi ijq/J)$, with $J/2 < q \leqslant J$, the mode is incorrectly represented as $\exp(2\pi ij(q-J)/J)$. This misinterpretation of Fourier modes in discrete systems is referred to as aliasing. An examination of quadratic interactions of Fourier modes, with attention paid to the aliasing property, enables one to represent exactly the semi-discrete form of (1.1) in terms of a system of ordinary differential equations describing the variation in time of a small number, say $N$, of Fourier coefficients. Briggs *et al.* produced exact representations involving one, two, three and four Fourier modes, and each of these is exact in the sense that no additional Fourier modes are introduced to the system by nonlinear interactions. It is convenient here to regard the lowest wave number occurring in any one of these representations as the analogue of the fundamental wave number in the periodic wavetrain considered by Benjamin and Feir [2].

If solutions of (1.1) are considered which are perturbations about a constant state characterised by a parameter $\alpha$ and if the initial energy in the perturbation is characterised by a parameter $E$, it is possible to find regions in $(\alpha, E)$ space within which the leap-frog solution of the $N$-mode ordinary differential system is stable. In such a region the midpoint (leap-frog) solution of the $N$-mode ordinary differential system should match the appropriate leap-frog solution of (1.1). Briggs *et al.* demonstrated, however, that the leap-frog solution of (1.1) containing $N$ Fourier modes is unstable to nonlinear interactions with Fourier modes which are side-bands in wavenumber space to the $N$ primary modes. The side-band modes, which cannot be represented by the discretised $N$-mode ordinary difference system, are triggered by roundoff errors in the leap-frog discretisation of (1.1). The side-band modes are then amplified by nonlinear interactions and the instability appears as a distortion of the envelope of the $N$ primary modes. This distortion develops and eventually the numerical solution becomes unbounded. Numerical results of Briggs *et al.* show the instabilities for $N = 2$ and $N = 3$. The authors used Fourier analysis of the numerical solution to illustrate the initial growth of certain side-band modes and they have derived envelope equations which purport to describe the initial growth in amplitude of the envelope modulation. Suggestions have been made by the authors concerning steps which might be taken to inhibit the nonlinear instabilities.

In this note we consider the stability of leap-frog solutions which contain one or two primary modes. Stability of the one-mode ordinary differential system is

examined and appropriate comparisons are made with the early work by Fornberg [4] on this one-mode case. Linear equations are derived which describe the first order interactions of side-bands, and numerical results show the envelope modulations produced by the side-band growth. Numerical experiments show that the growth rate of a side-band mode varies with the separation, in wave number space, between the side-band and the primary mode. The experiments suggest that there is a maximum growth rate associated with a particular value of this separation. A simplified analysis of the side-band equations indicates that there is a cut-off value in the wave number separation: if the gap between the primary mode and the side-band exceeds this cut-off then the side band will not grow as time evolves. Finally it is shown that side-band growth does not occur if (1.1) is integrated using a discretisation which conserves energy.

## 2. Difference Equations and $N$-Mode Equations

### 2.1. *Difference Equations*

Following Briggs *et al.* [3] we consider the equation

$$u'_t + (u' + U)\, u'_x = 0 \tag{2.1}$$

in a perturbation $u'(x, t)$ about a constant solution $u = U$ $(U > 0)$ of (1.1). We assume that $u'(x, t)$ satisfies the periodicity condition

$$u'(x + 1, t) = u'(x, t) \tag{2.2}$$

and we examine numerical solutions on a discretisation of the region $D = \{(x, t)$: $0 \leqslant x \leqslant 1,\ t \geqslant 0\}$ using a time step $k$ and a space step $h = 1/J$, where $J$ is an even integer. The approximation $U_j^n$ to $u'(jh, nk)$ is formed using the leap-frog scheme

$$U_j^{n+1} - U_j^{n-1} + \frac{\theta\gamma}{2}\left[(U_{j+1}^n)^2 - (U_{j-1}^n)^2\right] + \left[(1-\theta)\,\gamma U_j^n + \alpha\right]\left[U_{j+1}^n - U_{j-1}^n\right] = 0, \tag{2.3}$$

where $\gamma = k/h$, $\alpha = \gamma U$ and the real parameter $\theta$ satisfies the constraint $0 \leqslant \theta \leqslant 1$. Scheme (2.3) is used for $1 \leqslant j \leqslant J$, $n \geqslant 1$, and the periodicity condition is incorporated in the form

$$U_0^{n+1} = U_J^{n+1}, \qquad U_{J+1}^{n+1} = U_1^{n+1} \tag{2.4}$$

Briggs *et al.* noted that (2.3) and (2.4) satisfy the invariance condition

$$\sum_{j=1}^{J} U_j^{n+1} = \sum_{j=1}^{J} U_j^{n-1}, \qquad n \geqslant 1, \tag{2.5}$$

for any $\theta \in \mathbb{R}$ and the additional condition

$$\sum_{j=1}^{J} U_j^n U_j^{n+1} = \text{constant}, \qquad n \geqslant 0, \tag{2.6}$$

for the choice $\theta = \frac{2}{3}$. This latter condition led the authors to assume the value $\theta = \frac{2}{3}$ in all computations using (2.3) and they also set $\gamma = 1$ to reduce the selection of parameters.

It is readily shown that $U_j^n = \xi^n \exp(2\pi ijp/J)$, $0 \leqslant p \leqslant J/2$, is a stable solution of the linear portion of (2.3) if

$$\alpha \leqslant [\sin(2\pi p/J)]^{-1} = \alpha_p.$$

In this case $\xi^n$ may be written as $\exp(-in\phi)$ and $\phi \in \mathbb{R}$ assumes one of the values

$$\phi_1 = \arctan\left[\frac{\alpha \sin(2\pi p/J)}{\sqrt{(1-\alpha^2 \sin^2(2\pi p/J))}}\right], \qquad \phi_2 = \pi - \phi_1. \tag{2.7}$$

The existence of two values of $\phi$ is associated with the two-step time discretisation and it is readily shown that the $\phi_1$ mode converges to the differential solution as $h \to 0$ ($J \to \infty$, $p$ constant). A plot of $\alpha_p$ against $p$ produces the neutral stability curve in the $(p, \alpha)$ plane and the location of the minimum on the curve shows that the mode with wavelength $4h$, corresponding to $p = J/4$, is the least stable mode in the linear problem. This mode, and therefore every mode, is stable if $\alpha \leqslant 1$. This is effectively the von Neumann stability condition for the linear problem.

### 2.2. *N-Mode Equations for* $N = 1, 2$

The semi-discrete form of (2.1) may be written as

$$\dot{U}_j + \frac{\theta}{4h}[(U_{j+1})^2 - (U_{j-1})^2] + \frac{1}{2h}[(1-\theta)\, U_j + U][U_{j+1} - U_{j-1}] = 0, \tag{2.8}$$

where $U_j(t)$ is an approximation to $u'(jh, t)$ and the dot denotes differentiation with respect to $t$. It is readily shown that (2.8) has a solution of the form

$$U_j(t) = A(t) \exp(2\pi ij/3) + A^*(t) \exp(-2\pi ij/3) \tag{2.9}$$

provided $A(t)$ and its complex conjugate $A^*(t)$ satisfy

$$\dot{A}(t) + \frac{i\sqrt{3}U}{2h} A(t) = \frac{i\sqrt{3}}{4h}(2-3\theta)\, A^{*2}(t). \tag{2.10}$$

A leap-frog discretisation of (2.10) yields the ordinary difference equation

$$A(n+1) - A(n-1) + i\sqrt{3}\alpha\, A(n) = \frac{i\sqrt{3}}{2}\gamma(2-3\theta)\, A^{*2}(n), \tag{2.11}$$

where $A(n)$ is an approximation to $A(t)$ at $t=nk$. This is the 1-mode equation given by Briggs *et al.* [3]. The existence of the 1-mode solution derives from the fact that spatial modes of the form $\exp(\pm 4\pi ij/3)$ produced by the quadratic nonlinearity are indistinguishable from $\exp(\mp 2\pi ij/3)$, respectively, due to the aliasing property. Note that the 1-mode system is linear if $\theta = 2/3$.

Equation (2.8) has a solution of the form

$$U_j(t) = A(t)\exp(\pi ij/2) + A^*(t)\exp(-\pi ij/2) + B(t)\exp(\pi ij), \tag{2.12}$$

provided the complex function $A(t)$ and the real function $B(t)$ satisfy

$$\dot{A}(t) + \frac{iU}{h}A(t) = \frac{i}{h}(1-2\theta)\,A^*(t)\,B(t) \tag{2.13a}$$

and

$$\dot{B}(t) = \frac{i}{h}(\theta-1)[A^2(t) - A^{*2}(t)]. \tag{2.13b}$$

A leap-frog discretisation of (2.13) yields

$$A(n+1) - A(n-1) + i2\alpha A(n) = i2\gamma(1-2\theta)\,A^*(n)\,B(n), \tag{2.14a}$$

and

$$B(n+1) - B(n-1) = i2\gamma(\theta-1)[A^2(n) - A^{*2}(n)], \tag{2.14b}$$

which is the 2-mode system given by Briggs *et al.* [3]. Note that the 2-mode system is linear if $\theta = 1$. There is no value of $\theta$ which gives linearisation for $N > 2$.

## 3. Stability of $N$-Mode Equations

We are interested in examining nonlinear instabilities of (2.3) and (2.4) in regions of parameter space in which the $N$-mode ordinary difference equations (2.11) and (2.14) are stable. To this end we obtain the nonlinear stability threshold of the $N$-mode equations. In the case of the 1-mode system a precise description of the nonlinear stability limit may be obtained for the differential equation (2.10). If $A(t) = X(t) + iY(t)$, with $X$ and $Y$ real, Eq. (2.10) may be written as

$$\begin{aligned} \dot{X} &= LY + 2MXY \\ \dot{Y} &= -LX + M(X^2 - Y^2), \end{aligned} \tag{3.1}$$

where $L = (\sqrt{3}/2)(U/h)$ and $M = (\sqrt{3}/4h)(2-3\theta)$. If $M \neq 0$ system (3.1) has singular points at $(0, 0)$, $(L/M, 0)$, $(-L/2M, \pm\sqrt{3}L/2M)$ on the $(X, Y)$ plane. It is readily shown that the singular point at the origin is a centre and that the other

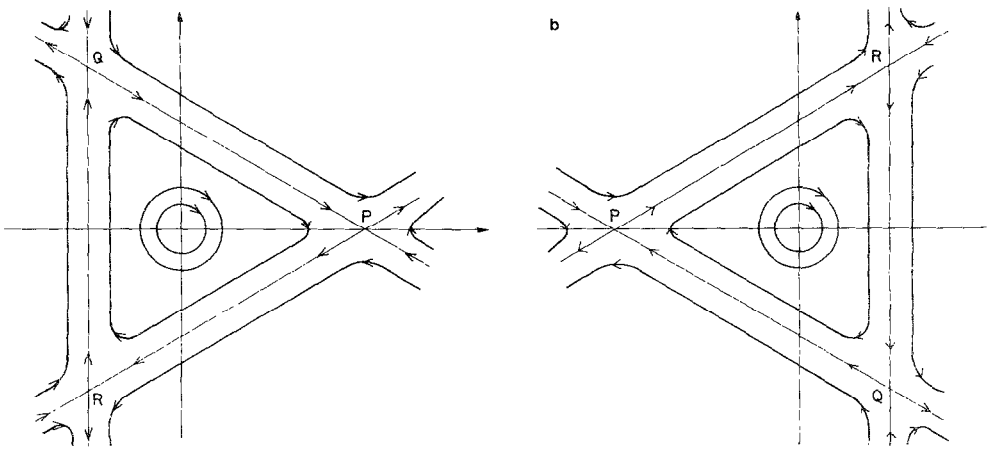


FIG. 1. Stability of 1-mode system. (a), (b) Integral curve patterns for $M>0$ and $M<0$.

singular points are saddle points. The integral curve patterns for $M>0$ and $M<0$ are shown in Figs. 1a and b, respectively. The lines $X=-L/2M$ and $X\pm\sqrt{3}Y=L/M$ which form triangle $PQR$ are integral curves of (3.1). The figures show that the solution of (3.1) or (2.10) will remain bounded for all $t>0$ if the initial point is inside triangle $PQR$. In theory a solution will also remain bounded if the initial point is on the triangle boundary, or on those extensions of the boundary lines on which the arrow-heads are directed towards the triangle. Infinitesimal perturbations of these solutions are unstable and we therefore discard such initial points. The stability region of (3.1) or (2.10) is the interior of triangle $PQR$ in Fig. 1. Note that the region covers the complete $(X, Y)$ plane if $\theta=\frac{2}{3}$.

Before considering the discrete 1-mode equations it is of interest to compare the analysis of (3.1) with results obtained by Fornberg [4] on instabilities in discretisations of (1.1) He considered perturbations about a zero state described by initial data with nodal values $\{\ldots, 0, -\kappa, \kappa, 0, -\kappa, \kappa, 0, \ldots\}$, where $\kappa\neq 0$. His solutions may be generated by the 1-mode equations above if we set $X\equiv 0$ and assume $U=0$. In this case the solution of (3.1) is

$$Y(t)=\frac{1}{Mt+1/Y(0)}$$

and, if $\theta\neq\frac{2}{3}$, this solution becomes unbounded at $t=-1/MY(0)$ provided $Y(0)$ is chosen such that $MY(0)<0$.

If Fornberg's initial data set is generalised to include perturbations about zero by any data with spatial frequency $3h$ we have a system described by (3.1) with $L\equiv 0$. If $\theta\neq\frac{2}{3}$ this system has one singular point at $(0, 0)$ and the integral curves satisfy the equation

$$X(X^2-3Y^2)=\text{constant}.$$

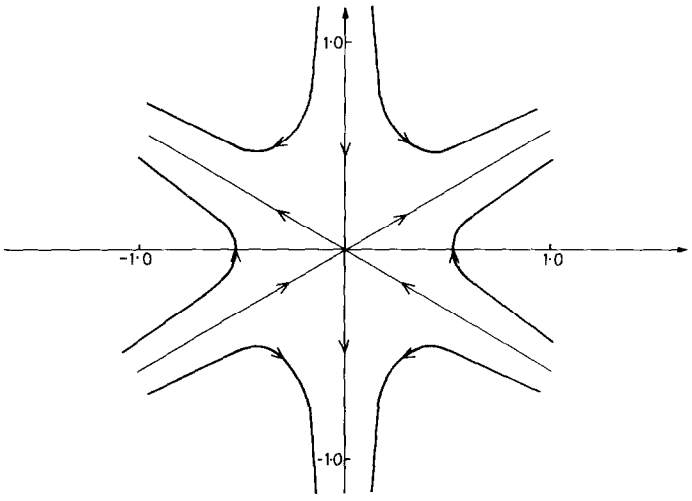


FIG. 2. Stability of 1-mode system. Integral curve pattern for $L=0$, $M>0$.

Figure 2 shows the solution trajectories if $M>0$. The case $M<0$ is obtained by reversing the arrow-heads on the trajectories. Fornberg's solution from the initial data set $\{..., -\kappa, \kappa, 0, -\kappa, \kappa, 0,...\}$ is described by the trajectory on $X=0$ in Fig. 2. If $\theta<\frac{2}{3}$ then $M>0$ and the solution with $Y(0)<0$ becomes unbounded in a finite time. This solution is represented by the trajectory $X=0$, $Y<0$ in Fig. 2 and it is readily shown to be the solution from the above initial data set with $\kappa<0$. Note that the trajectory $X=0$, $Y<0$ takes the shortest path to infinity, suggesting that this might be the least stable 1-mode solution. Similarly we note that if $\theta>\frac{2}{3}$ then $M<0$ and the trajectory which moves directly to infinity is represented by $X=0$, $Y>0$. This is the solution which arises from the Fornberg data set with $\kappa>0$.

Leap-frog instabilities associated with $U=0$ have also been examined by Trefethen [9] and Vadillo and Sanz-Serna [10]. Trefethen has shown by numerical experimentation that a local sign change of the form $U_j>0$, $U_{j+1}<0$ is amplified catastrophically if $\theta<\frac{2}{3}$, and that a sign change $U_j<0$, $U_{j+1}>0$ is amplified—albeit less severely—if $\theta>\frac{2}{3}$. Sign changes of this type arise from the Fornberg data set with $\kappa<0$ and $\kappa>0$, respectively, and $U_j=-\kappa$. Vadillo and Sanz-Serna [10] have shown that for $\theta=0$ the least stable solution of the fully discrete leap-frog equation is a solution of the form $U_l=\kappa$, $U_{l+1}=-\kappa$, $U_j=0$ if $j\neq l$, $l+1$: here $l$ is a positive integer and $\kappa$ is a positive real number. Vadillo and Sanz-Serna have conducted numerical experiments to support their analysis.

The work cited in the two preceding paragraphs deals with instabilities associated with perturbations about the zero solution. If $U\neq 0$ and perturbations are not too large then local sign changes do not occur and the solutions are more stable. The interesting work by Briggs, Newell and Sarie [3] on nonlinear focusing describes a mechanism which might lead to the destabilisation of "stable" solutions when

TABLE I

Stability Threshold for the 1-Mode Difference Equation with $\gamma = 1$ and $\theta = 0$

| $\alpha$ | 0 | 0.1 | 0.2 | 0.3 | 0.4 | 0.5 | 0.6 | 0.7 | 0.8 | 0.9 | 1.0 |
|---|---|---|---|---|---|---|---|---|---|---|---|
| $E$ | 0 | 0.10 | 0.10 | 0.20 | 0.25 | 0.30 | 0.30 | 0.30 | 0.30 | 0.20 | 0 |

$U \neq 0$. Henceforth we confine our attention to the case $U \neq 0$, and our aim is to add to the work by Briggs *et al.*

For the case $U \neq 0$ the integral curve patterns in Fig. 1 for the 1-mode differential equation offer some guidance concerning the stability region for the nonlinear difference equation (2.11). A requirement for stability is that the discrete approximations $A(0)$, $A(1)$, $A(2)$,... should remain inside triangle $PQR$ in Fig. 1. To determine the stability threshold, however, we solved (2.11) with $\gamma = 1$ and $\theta = 0$ using starting values $A(0) = A(1) = \sigma(1 + i)$, where $\sigma$ is a positive constant and $(\sigma, \sigma)$ is in triangle $PQR$. $\theta = 0$ was chosen as the value of $\theta$ which minimises the area of the stability region $PQR$. It follows from (2.9) that the nodal values of the perturbation are

$$\{U_0(0), U_1(0),...\} = \sigma\{2, -(\sqrt{3}+1), (\sqrt{3}-1), 2,...\}. \tag{3.2}$$

The maximum norm of this data set is

$$E = \sigma(\sqrt{3}+1) \tag{3.3}$$

and we employ $E$ as a parameterisation of the initial perturbation energy. To obtain the stability limit for a particular value of $\alpha$, Eq. (2.11) was integrated using increasing values of $E$ until we found the maximum $E$ at which the solution remained bounded over $2 \times 10^4$ integration steps. Table I gives the stability threshold obtained in this way. $E$ was increased in increments of 0.05, and a non-zero entry such as 0.20 indicates that the stability threshold is in the interval (0.20, 0.25). The zero values at $\alpha = 0$ and $\alpha = 1$ are precise: the value $\alpha = 0$ has been dealt with in the discussion of Fig. 2, and $\alpha = 1$ is the linear stability limit. As one might expect, the choice of starting value $A(1)$ has some effect on the stability threshold for the discrete problem. One of the solutions of the linear part of (2.11) could be used to determine $A(1)$. With $A(1) = A(0)\exp(-i\phi)$, and $\phi$ given by (2.7), we found with $\alpha = 0.9$, for example, that the threshold value is slightly increased for $\phi = \phi_1$ and slightly decreased for $\phi = \phi_2$.

To determine the stability threshold for the 2-mode problem we solved (2.14) with $\gamma = 1$ and $\theta = \frac{2}{3}$ using starting values $A(0) = A(1) = \sigma(1 + i)$, $B(0) = B(1) = \sigma$, where $\sigma$ is a positive constant. This data set was used by Briggs *et al.* [3] for the 2-mode problem. In this case Eq. (2.12) gives the nodal values of the initial perturbation as

$$\{U_0(0), U_1(0),...\} = \sigma\{3, -3, -1, 1, 3, -3,...\} \tag{3.4}$$

TABLE II

Stability Threshold for the 2-Mode Difference Equation with $\gamma = 1$ and $\theta = \frac{2}{3}$

| $\alpha$ | 0 | 0.1 | 0.2 | 0.3 | 0.4 | 0.5 | 0.6 | 0.7 | 0.8 | 0.9 | 1.0 |
|---|---|---|---|---|---|---|---|---|---|---|---|
| $E$ | 0 | 0.90 | 1.45 | 1.65 | 1.70 | 1.25 | 1.15 | 1.15 | 0.80 | 0.40 | 0 |

and the perturbation energy may be measured by

$$E = 3\sigma. \tag{3.5}$$

The threshold values given in Table II were computed as for the 1-mode problem with $E$ once more increased in increments of 0.05. As for the 1-mode system, the threshold values are marginally altered if $A(1)$ and $B(1)$ are evaluated using solutions of the linear part of (2.14).

## 4. Side-Band Equations

Consider a solution of the semi-discrete equation (2.8) represented by the 1-mode system (2.9). The solution may be considered to be the analogue of a periodic wavetrain in deep water with fundamental wave number $2\pi J/3$. In this discrete system the higher harmonics in the wavetrain are reflected into the fundamental by the aliasing property. Suppose the solution is perturbed by the presence of Fourier components with wave number close to the fundamental of the form $(2\pi/3 + \delta) J$, where $\delta J = 2\pi\mu$ and $\mu$ is typically a small positive integer. The side-bands are conveniently represented by

$$a_+(t)\, e^{i(\rho+\delta)j} + a_+^*(t)\, e^{-i(\rho+\delta)j},$$

where $\rho = 2\pi/3$, and $|a_+(0)/A(0)|$ is assumed to be sufficiently small to permit the neglect of squares and higher powers of $a_+(t)$ for some initial period of time. Quadratic interactions between the term in $a_+(t)$ and the fundamental terms in (2.9) give rise to first order terms with spatial distributions of the form $e^{i(2\rho+\delta)j} = e^{-i(2\rho-\delta)j}$ and $e^{i\delta j}$. In this context a first order term is a term containing first powers of small quantities such as $a_+(t)$. An examination of all possible interactions between the fundamental terms and the side-bands reveals that the solution containing all fundamental and first order terms may be written as

$$\begin{aligned} U_j = {} & Ae^{i\rho j} + A^* e^{-i\rho j} + a_-\, e^{i(\rho-\delta)j} + a_-^*\, e^{-i(\rho-\delta)j} + a_+\, e^{i(\rho+\delta)j} \\ & + a_+^*\, e^{-i(\rho+\delta)j} + be^{i\delta j} + b^* e^{-i\delta j}. \end{aligned} \tag{4.1}$$

The argument $t$ has been omitted from the coefficients in (4.1) for notational convenience. Note here that an upper side-band containing $e^{i(\rho+\delta)j}$ interacts with the

fundamental mode to produce a lower side-band term containing $e^{-i(\rho-\delta)t}$. This interaction between upper and lower side-bands through the fundamental mode arises from the aliasing property, and it is not produced by the quadratic non-linearity $uu_x$ in a periodic wavetrain. In a periodic wavetrain the upper and lower side-bands of the first harmonic interact through the second harmonic [1].

If we substitute (4.1) into (2.8), ignore squares of small terms such as $a_+(t)$, and use a discrete orthogonality condition on the spatial components, we obtain the differential system

$$\dot{a}_- + \frac{Ui\sin(\rho-\delta)}{h} a_- + \frac{(1-\theta)\,i}{h}[Ab^*(\sin\rho - \sin\delta) - A^*a_+^*(\sin\rho + \sin(\rho+\delta))]$$
$$+ \frac{\theta i}{h}\sin(\rho-\delta)(Ab^* + A^*a_+^*) = 0,$$
$$\dot{a}_+ + \frac{Ui\sin(\rho+\delta)}{h} a_+ + \frac{(1-\theta)\,i}{h}[Ab(\sin\rho + \sin\delta) - A^*a_-^*(\sin\rho + \sin(\rho-\delta))]$$
$$+ \frac{\theta i}{h}\sin(\rho+\delta)(Ab + A^*a_-^*) = 0,$$
$$\dot{b} + \frac{Ui\sin\delta}{h} b + \frac{(1-\theta)\,i}{h}[Aa_-^*(\sin\rho - \sin(\rho-\delta)) - A^*a_+(\sin\rho - \sin(\rho+\delta))]$$
$$+ \frac{\theta i}{h}\sin\delta(Aa_-^* + A^*a_+) = 0. \tag{4.2}$$

In all 1-mode computations we set $\theta = 0$, this being the value which minimises the stability region $PQR$ in Fig. 1. In this case the side-band differential system is

$$\begin{aligned} \dot{a}_- + iF(\delta)\,a_- + i(K(\delta)\,Ab^* - M(\delta)\,A^*a_+^*) &= 0, \\ \dot{a}_+ + iF(-\delta)\,a_+ + i(K(-\delta)\,Ab - M(-\delta)\,A^*a_-^*) &= 0, \\ \dot{b} + iL(\delta)\,b + i(N(\delta)\,Aa_-^* - N(-\delta)\,A^*a_+) &= 0, \end{aligned} \tag{4.3}$$

where

$$F(\delta) = \frac{U}{2h}(\sqrt{3}\cos\delta + \sin\delta), \qquad K(\delta) = \frac{1}{h}\left(\frac{\sqrt{3}}{2} - \sin\delta\right),$$
$$M(\delta) = \frac{1}{2h}(\sqrt{3} + \sqrt{3}\cos\delta - \sin\delta), \qquad N(\delta) = \frac{1}{2h}(\sqrt{3} - \sqrt{3}\cos\delta - \sin\delta)$$

and

$$L(\delta) = \frac{U}{h}\sin\delta.$$

The fundamental coefficient, $A(t)$, is altered by quadratic terms in the side-band coefficients and, if such terms are neglected, $A(t)$ is given by equation (2.10). Note also that quadratic terms introduce additional Fourier modes with wave numbers such as $(2\pi/3 \pm 2\delta)J$. If some mechanism permits $a_-, a_+$ and $b$ to grow until squares of these terms are significant then $A(t)$ is affected and energy will be transferred to additional Fourier modes. This process of energy cascade will be repeated and additional modes will be stimulated.

Before we consider the system (4.3) in more detail a simple interpretation should be given of the effect of the side-bands on the fundamental solution. If we ignore the coefficient $b(t)$ in (4.1) the solution at a given value of $t$ is

$$U_j = 2\,\mathrm{Re}[e^{ip j}(A + a_+ e^{i\delta j} + a_- e^{-i\delta j})],$$

where Re denotes the real part. This may be written as

$$U_j = 2\{[X + \mathscr{F}(j)]\cos(2\pi j/3) - [Y + \mathscr{G}(j)]\sin(2\pi j/3)\}, \tag{4.4}$$

where $A = X + iY$ and $\mathscr{F}(j)$ and $\mathscr{G}(j)$ are first order linear combinations of $\cos \delta j$ and $\sin \delta j$. Since $\mathscr{F}(j)$ and $\mathscr{G}(j)$ are periodic functions with period $2\pi/\delta J = 1/\mu$ it follows that the side-bands introduce a modulation so that the constant envelope is replaced by a periodic function with wavelength $1/\mu$. Th reader is referred to the text by Whitham [11] for a description of modulation theory applied to water waves and nonlinear dispersive waves.

In an attempt to obtain a condition for the existence of growing solutions of the semi-discrete system (4.3) we use an analysis based on a two-fold simplification of the differential system. Suppose initially that $A(t)$ is given by the linear part of (2.10) as

$$A(t) = a_0 e^{-i\omega t}, \tag{4.5}$$

where $\omega = \sqrt{3}\,U/2h$. This solution might be regarded as a circular trajectory around the centre, within triangle $PQR$, in Fig. 1. With this simplification (4.3) becomes

$$\begin{aligned} \dot{a}_- + iF(\delta)\,a_- + i(K(\delta)\,a_0 b^* e^{-i\omega t} - M(\delta)\,a_0^* a_+^* e^{i\omega t}) &= 0, \\ \dot{a}_+ + iF(-\delta)\,a_+ + i(K(-\delta)\,a_0 b e^{-i\omega t} - M(-\delta)\,a_0^* a_-^* e^{i\omega t}) &= 0, \\ \dot{b} + iL(\delta)\,b + i(N(\delta)\,a_0 a_-^* e^{-i\omega t} - N(-\delta)\,a_0^* a_+ e^{i\omega t}) &= 0. \end{aligned} \tag{4.6}$$

To further simplify the system we set $b(t)$ to zero and obtain the equations

$$\begin{aligned} \dot{a}_- + iF(\delta)\,a_- - iM(\delta)\,a_0^* a_+^* e^{i\omega t} &= 0, \\ \dot{a}_+ + iF(-\delta)\,a_+ - iM(-\delta)\,a_0^* a_-^* e^{i\omega t} &= 0, \end{aligned} \tag{4.7}$$

in $a_-$ and $a_+$. The elimination of $a_+$ from (4.7) yields

$$\ddot{a}_- + i[F(\delta) - F(-\delta) - \omega]\,\dot{a}_- - [M(\delta)\,M(-\delta)|a_0|^2 - \omega F(\delta) - F(\delta)\,F(-\delta)]\,a_- = 0.$$

This equation has a solution of the form $a_- = e^{i\lambda t}$ if and only if

$$\lambda^2 + [F(\delta) - F(-\delta) - \omega]\,\lambda + [M(\delta)\,M(-\delta)|a_0|^2 - \omega F(\delta) - F(\delta)\,F(-\delta)] = 0.$$

and the condition for a growing solution is that the discriminant of this quadratic be negative. The condition may be reduced to

$$(3 - 4\eta^2)\cos^2\delta + (3 - 6\eta^2)\cos\delta + \tfrac{1}{4}(3 - 8\eta^2) < 0, \tag{4.8}$$

where $\eta = |a_0|/U$. Since $\rho = 2\pi/3$ and $(\rho + \delta) \leqslant \pi$ we see that $\delta \leqslant \pi/3$ so $\cos\delta > 0$. The condition for the circular trajectory (4.5) to be inside triangle $PQR$ in Fig. 1 is $\eta < \frac{1}{2}$. With these constraints imposed condition (4.8) cannot be satisfied and we might conclude that the semi-discrete 1-mode system does not permit side-band growth of the type described above.

One might be suspicious of conclusions on side-band growth which have been formulated in terms of the simplified model (4.7). To determine possible limitations on the conclusions we examine the nature of the solution of system (4.6). We have seen in (4.4) that modulation of the 1-mode system in space arises from the presence of periodic functions with periods $3h$ and $1/\mu$. The solution also evolves in time with variations which depend on two different time scales. To accentuate the disparity between the time scales consider the limiting form of (4.6) as $h \to 0$ with $\mu$ fixed. In the limit the system becomes

$$\begin{aligned} \dot{a}_- + i\omega a_- + i\omega(\alpha_0 b^* e^{-i\omega t} - 2\alpha_0^* a_+^* e^{i\omega t}) &= 0, \\ \dot{a}_+ + i\omega a_+ + i\omega(\alpha_0 b e^{-i\omega t} - 2\alpha_0^* a_-^* e^{i\omega t}) &= 0, \\ \dot{b} + 2i\Omega b - i\Omega(\alpha_0^* a_+ e^{i\omega t} + \alpha_0 a_-^* e^{-i\omega t}) &= 0, \end{aligned} \tag{4.9}$$

where $\alpha_0 = a_0/U$, $\omega = \sqrt{3}\,U/2h$ and $\Omega = \pi\mu U$. Since $\omega \gg 1$ we may introduce fast and slow time scales

$$T = \omega t \qquad \text{and} \qquad \tau = \Omega t$$

and expand $a_\pm$ and $b$ as

$$a_\pm = a_\pm^{(0)}(T, \tau) + O(h), \qquad b = b^{(0)}(T, \tau) + O(h).$$

The governing equations for the leading terms in the expansions are readily obtained using the method of multiple scales. The equation in $b^{(0)}$ is $\partial b^{(0)}/\partial T = 0$,

and if we drop the superscripts on $a_{\pm}^{(0)}$ and $b^{(0)}$ we may write the equations in $a_{-}^{(0)}$ and $a_{+}^{(0)}$ as

$$\dot{a}_- + ia_- + i(\alpha_0 b^* e^{-iT} - 2\alpha_0^* a_+^* e^{iT}) = 0,$$
$$\dot{a}_+ + ia_+ + i(\alpha_0 b e^{iT} - 2\alpha_0^* a_-^* e^{iT}) = 0,$$

where the dot denotes differentiation with respect to $T$ and $b = b(\tau)$. The solution of this system is

$$a_- = C_1(\tau)\, e^{i\lambda_1 T} + C_2(\tau)\, e^{i\lambda_2 T} + \frac{3\alpha_0 b^*}{4|\alpha_0|^2} e^{-iT} + \frac{\alpha_0^* b^*}{2\alpha_0} e^{2iT},$$

$$a_+ = \frac{(1+\lambda_1)}{2\alpha_0} C_1^*(\tau)\, e^{i\lambda_2 T} + \frac{(1+\lambda_2)}{2\alpha_0} C_2^*(\tau)\, e^{i\lambda_1 T} + \frac{3\alpha_0 b}{4|\alpha_0|^2} e^{-iT} + \frac{\alpha_0^* b}{2\alpha_0} e^{2iT},$$

where $C_1(\tau)$ and $C_2(\tau)$ are arbitrary functions and $\lambda_{1,2} = \frac{1}{2}[1 \pm (9 - 16|\alpha_0|^2)^{1/2}]$. Note that the roots of the quadratic equation which yielded (4.8) have the limiting values $\omega\lambda_1$ and $\omega\lambda_2$ as $h \to 0$.

The solution shows that $b(t)$ varies on the slow time scale whereas $a_{\pm}(t)$ oscillate on the fast time scale and they are modulated on the slow time scale with modulations determined by $C_1(\tau)$ and $C_2(\tau)$. Instability will not develop on the slow time scale if $C_1(\tau)$ and $C_2(\tau)$ remain bounded as $\tau$ evolves. This suggests that the approximation $b(t) \equiv 0$ in (4.7), which removes the slow time scale, will not detect any slowly developing modulational instability. Equations for $C_1(\tau)$ and $C_2(\tau)$ are produced by the removal of secular terms from the equations which govern the next terms in the expansions of $a_{\pm}(T, \tau)$ and $b(T, \tau)$. Rather than solve for $C_{1,2}$ we computed accurate numerical solutions of the side-band equations. In checking numerically for modulational instability care has to be taken to integrate over a sufficiently large range of the slow time scale. The third equation in (4.9) suggests that the slow variation of $b$ is a periodic variation in the variable $t$ with period $\pi/\Omega$ or $1/\mu U$. It is therefore essential to integrate over several multiples of $1/\mu U$. Note also that in order to construct an accurate representation of the solution it is essential to compute the solution at several points within each cycle of the fast time scale oscillation.

We integrated system (4.6) with $\delta$ and $\omega$ defined by the parameter values $J = 120$, $\mu = 3$ and $U = 0.9$. It is readily shown that for this set of values inequality (4.8) is satisfied if $|a_0| > 0.672$, and with $a_0 = \sigma(1+i) = E(1+i)/(1+\sqrt{3})$ this suggests that growth will occur if $E > 1.3$. System (4.6) was integrated from $t = 0$ to $t = 3.4$ by a Runge–Kutta–Merson method using different values of $E$ and with initial conditions $a_+ = 0.5 \times 10^{-5} \times (1+i)$, $a_- = b = 0$. The numerical experiments indicated that $|a_{\pm}|$ did not grow unboundedly in time unless $E$ exceeded 1.3. If $E = 1.3$ the maximum value of $|a_+|$ over the interval $0 \leqslant t \leqslant 3.4$ is of the order $10^{-4}$, and if $E = 1.32$ the maximum value of $|a_+|$ has reached $10^{+8}$ at $t = 1.5$. Figure 3 shows the evolution in time of the real parts of $a_+$ and $b$ with $J$, $\mu$ and $U$ as given above and with $E = 0.2$. The diagram clearly shows the fast and slow time variations of $a_+$ and

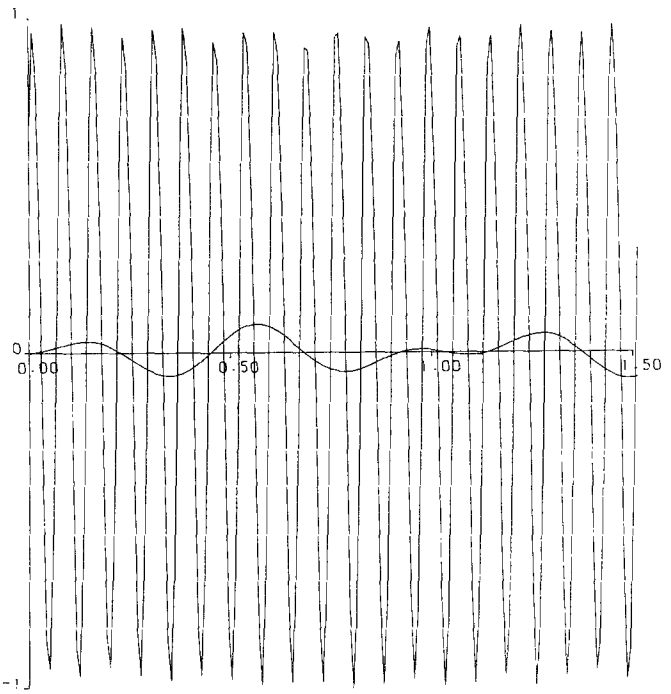


FIG. 3. Variation of real parts of $a_+$ and $b$ with time given by the accurate solution of system (4.6) with $E=0.2$, $J=120$, $\mu=3$ and $U=0.9$.

$b$, respectively. The numerical experiments suggest that, at least for the selected parameter set, the solution of (4.6) does not grow unboundedly if (4.8) is not satisfied.

To confirm that the complete semi-discrete 1-mode system (4.3) does not permit side-band growth if $A(t)$ is within triangle $PQR$ in Fig. 1 the system was integrated numerically with $J=120$, $\mu=3$, $U=0.9$ and $A(0)=E(1+i)/(1+\sqrt{3})$. This value of $A(0)$ is within triangle $PQR$ provided $E<U$. Using initial values on $a_-$, $a_+$ and $b$ as described in the preceding paragraph we found no growth in the maximum value of $|a_+|$ over the interval $0\leqslant t\leqslant 3.4$ provided $E<0.9$. At $E=0.9$, however, the solution grows rapidly with time. The numerical experiments suggest that the semi-discrete 1-mode system does not permit side-band growth.

We now consider the discretisation of the side-band equations by the midpoint rule. If the side-band modes are small then the solution of (4.3) by this discretisation could equally be obtained by Fourier decomposition of appropriate leap-frog solutions of (2.1). If $b(t)$ is set to zero, as in (4.7), the midpoint discretisation of (4.3) gives

$$\begin{aligned} \Delta_0 a_-(n)+iF(\delta)\,a_-(n)-iM(\delta)\,A^*(n)\,a_+^*(n)=0,\\ \Delta_0 a_+(n)+iF(-\delta)\,a_+(n)-iM(-\delta)\,A^*(n)\,a_-^*(n)=0, \end{aligned} \tag{4.10}$$

where $\Delta_0 a_-(n) = [a_-(n+1) - a_-(n-1)]/2k$. If $A(n)$ is assumed to be one of the solutions of the linear part of (2.11) then

$$A(n) = a_0 e^{-i\phi n}, \tag{4.11}$$

where $\phi$ is $\phi_1$ or $\phi_2$ in (2.7), with $p$ set to $J/3$. It is possible to eliminate $A(n)$ and $a_+(n)$ from Eq. (4.10) and (4.11). The elimination process makes use of the identity

$$\Delta_0[e^{i\phi n} a_+^*(n)] = e^{i\phi n}[\cos\phi\, \Delta_0 a_+^*(n) + \frac{i}{k} \sin\phi\, \langle a_+^*(n)\rangle],$$

where $\langle a_+^*(n)\rangle$ denotes $\frac{1}{2}[a_+^*(n+1) + a_+^*(n-1)]$. The final result is amenable to simple analysis if $\langle a_+^*(n)\rangle$ is replaced by $a_+^*(n)$ in this identity and, with this simplification incorporated, the final difference equation in $a_-(n)$ is

$$\Delta_0^2 a_-(n) + i\mathscr{H}\, \Delta_0 a_-(n) - \mathscr{K} a_-(n) = 0,$$

where $\mathscr{H} = F(\delta) - \cos\phi\, F(-\delta) - (1/k)\sin\phi$ and $\mathscr{K} = \cos\phi\; M(\delta)\; M(-\delta)|a_0|^2 - (1/k)\; \sin\phi\, F(\delta) - \cos\phi\, F(\delta)\, F(-\delta)$. This equation has a solution of the form $a_-(n) = r^n$ if and only if

$$\zeta^2 + i2k\mathscr{H}\zeta - 4k^2\mathscr{K} = 0, \tag{4.12}$$

where $\zeta = r - r^{-1}$. If $\phi$ is identified with $\phi_1$ in (2.7), and $\gamma = k/h = 1$, the coefficients in (4.12) are given by

$$2k\mathscr{H} = \alpha[(1-q)\sqrt{3}\cos\delta + (1+q)\sin\delta - \sqrt{3}]$$

and

$$4k^2\mathscr{K} = -\alpha^2\{3\cos\delta + \sqrt{3}\sin\delta + q[4\cos^2\delta - 1 - \eta^2(2 + 6\cos\delta + 4\cos^2\delta)]\},$$

where $q = \sqrt{(1 - \frac{3}{4}\alpha^2)}$ and $\eta = |a_0|/\alpha$. When $\phi$ is identified with $\phi_2$ in (2.7) then $q$ is replaced by $-q$ in the expressions for $\mathscr{H}$ and $\mathscr{K}$.

The discussion following (4.8) indicates that $\delta \leqslant \pi/3$ and that $E$ should be selected so that the unperturbed system is stable. Accordingly, we evaluated the four roots of (4.12) for $\alpha = 0.9$, $|a_0| = 0.1$ and $\delta = 0(\pi/15)\,\pi/3$. This value of $|a_0|$ corresponds to a value of $E$ just below the stability limit given in Table I. With $\phi = \phi_1$ the largest root of (4.12) has modulus 2.02, 1.83, 1.57, 1.04, 1, 1 at $\delta = 0(\pi/15)\,\pi/3$ and with $\phi = \phi_2$ the largest root has modulus 1 for all values of $\delta$. The existence of roots $r$ of (4.12) with $|r| > 1$ suggests that the fully discrete system may exhibit side-band growth at values of $\alpha$ and $E$ for which solutions of (2.11) are stable.

To check the effect of the aproximation $b(t) = 0$ in (4.10) the system (4.6) in $a_\pm$ and $b$ was integrated using the midpoint rule with $\gamma = k/h = 1$. Experiments were performed with $J = 120$, $U = 0.9$, $a_0 = E(1+i)/(1+\sqrt{3})$ and with conditions at

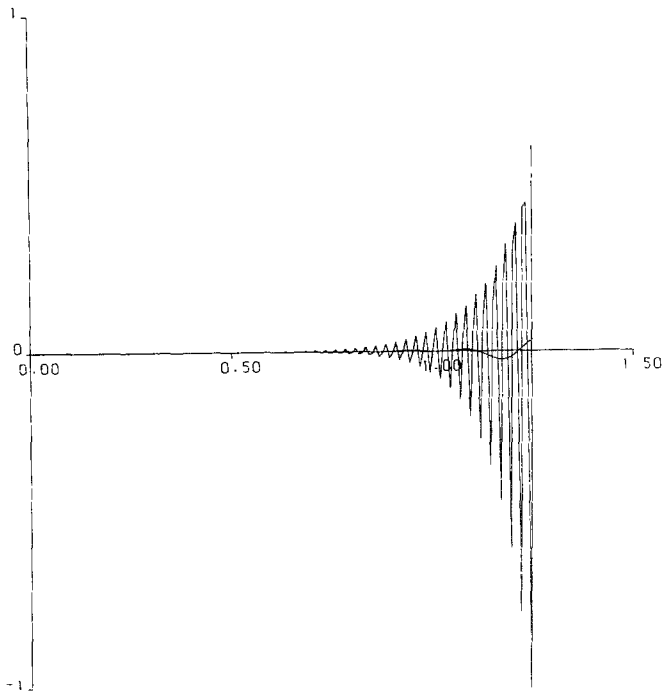


FIG. 4. Variation of real parts of $a_+$ and $b$ with time given by the midpoint rule solution of system (4.6) with $E=0.15$, $J=120$, $\mu=3$, $\gamma=1$ and $U=0.9$.

$n=0, 1$ defined by $a_+=0.5\times10^{-5}(1+i)$, $a_-=b=0$. Rapidly growing solutions were found for $\phi=\phi_1$ and $\phi=\phi_2$ at values of $E$ below the stability limit given by Table I. For example, Fig. 4 shows the evolution in time of the real parts of $a_+$ and $b$ with $\mu=3$ and $E=0.15$. The solution is shown for 150 time steps and it is scaled so that the maximum amplitude is unity. Over 150 time steps the value of $|a_+|$ increases to 4.0. Figure 4 shows the fast variation in $a_+$ and the slow variation in $b$. The plot of $a_+$ suggests a growth on the fast time scale.

Experiments were also performed on the midpoint rule discretisation of the complete 1-mode system (4.3). With $E$ below the stability limit of Table I the complete system exhibits side-band growth. Numerical results indicate that the initial rate of growth of $|a_\pm|$ varies with $\mu$ and that the growth rate is greatest when $\mu=J/6$, or $\delta=\pi/3$. It is of interest to note that Benjamin and Feir [2] obtained results of this type in their analysis of wavetrain instabilities in deep water.

In the case of the 2-mode system the solution containing all fundamental and first order terms may be written as

$$U_j=Ae^{i\pi j/2}+Be^{i\pi j}+a_-e^{i(\pi/2-\delta)j}+a_+e^{i(\pi/2+\delta)j}$$
$$+b_-e^{i(\pi-\delta)j}+de^{i\delta j}+\text{c.c.}, \tag{4.13}$$

where c.c. denotes the complex conjugates of the terms in $A$, $a_-$, $a_+$, $b_-$ and $d$. As before, $\delta J = 2\pi\mu$, and $\mu$ is typically a small positive integer. The differential system in the side-band coefficients is readily shown to be

$$\dot{a}_- + \frac{Ui\cos\delta}{h} a_- + \frac{(1-\theta)\,i}{h}\left[-\cos\delta\, Ba_+^* + (\sin\delta - 1)(A^* b_- - Ad^*)\right]$$

$$+ \frac{\theta i\cos\delta}{h}\left[Ba_+^* + A^* b_- + Ad^*\right] = 0,$$

$$\dot{a}_+ + \frac{Ui\cos\delta}{h} a_+ + \frac{(1-\theta)\,i}{h}\left[-\cos\delta\, Ba_-^* + (\sin\delta + 1)(Ad - A^* b_-^*)\right]$$

$$+ \frac{\theta i\cos\delta}{h}\left[Ba_-^* + A^* b_-^* + Ad\right] = 0,$$

$$\dot{b}_- + \frac{Ui\sin\delta}{h} b_- + \frac{(1-\theta)\,i}{h}\left[-\sin\delta\, Bd^* + (\cos\delta + 1)(Aa_- - A^* a_+^*)\right]$$

$$+ \frac{\theta i\sin\delta}{h}\left[Bd^* + A^* a_+^* + Aa_-\right] = 0,$$

$$\dot{d} + \frac{Ui\sin\delta}{h} d + \frac{(1-\theta)\,i}{h}\left[-\sin\delta\, Bb_-^* + (\cos\delta - 1)(A^* a_+ - Aa_-^*)\right]$$

$$+ \frac{\theta i\sin\delta}{h}\left[Bb_-^* + A^* a_+ + Aa_-^*\right] = 0. \tag{4.14}$$

In all 2-mode computations we set $\theta = \frac{1}{2}$ and the side-band equations (4.14) are modified accordingly. The presence of the side-bands introduces a modulation of wavelength $2\pi/\delta J = 1/\mu$. As before, the fundamental coefficients are not affected by first order terms in the side-band coefficients. If squares of these coefficients become significant then the fundamental coefficients are influenced and additional Fourier modes are stimulated.

Rather than impose severe simplifications on the 2-mode system (4.14) we attempted to investigate growth properties by means of numerical experiments. An accurate numerical solution was obtained with $J = 120$, $\mu = 3$ and $U = 0.9$. Values of dependent variables at $t = 0$ were given by $A = E(1+i)/3$, $B = E/3$, $a_+ = 0.5 \times 10^{-5} \times (1+i)$, $a_- = b_- = d = 0$. There was no noticeable growth in the maximum value of $|a_+|$ over the interval $0 \leqslant t \leqslant 2.9$ for $E < 1.0$. The system (4.14) was also integrated using the midpoint rule with $\gamma = 1$ and with the above initial conditions imposed at $n = 0, 1$. The fully discrete solution exhibited side-band growth at values of $E$ below the stability limit given in Table II. At $E = 0.4$, for example, $|a_+(n)|$ reaches $10^{+4}$ over 180 time steps. As in the 1-mode case the initial growth rate varies with $\mu$ and the growth appears to be greatest around $\mu = J/10$.

## 5. Numerical Results with the Partial Difference Equations

The relation between instabilities and side-band growth was examined using numerical integrations of the partial difference equations (2.3) and (2.4) for the 1-mode and 2-mode systems. The 1-mode system involved parameter values $\theta = 0$, $\gamma = 1$, $\alpha = 0.9$ and $E$ was chosen to satisfy $E \leqslant 0.2$ as dictated by the threshold results of Table I. $J$ has to be a multiple of 3 to permit the periodicity condition, and the selected values of $J$ were also even integers. Initial conditions are given by (3.2) with side-band disturbances added as required. For example, to stimulate mode number $p$, $0 \leqslant p \leqslant J/2$, we added

$$ce^{2\pi ijp/J} + c^* e^{-2\pi ijp/J} = 2\varepsilon[\cos(2\pi jp/J) - \sin(2\pi jp/J)] \tag{5.1}$$

to node $j$ for $j = 0, 1, \ldots$, where $c = \varepsilon(1 + i)$ and $\varepsilon$ is a small positive number. At time step $n$ in the integration process the Fourier coefficient associated with a typical mode $s$ is given by the transformation

$$U(s, nk) = \frac{1}{J} \sum_{j=0}^{J-1} U_j^n e^{-2\pi isj/J}, \qquad |s| \leqslant J/2,\ s \neq -J/2. \tag{5.2}$$

The 2-mode system involved parameter values $\theta = \frac{2}{3}$, $\gamma = 1$, $\alpha = 0.9$ and $E \leqslant 0.4$. In this case $J$ was chosen to be a multiple of 4.

The side-band modes $a_+$ in (4.1) and (4.13) were stimulated using (5.1), with $p = J/3 + \mu$ and $p = J/4 + \mu$ in the 1-mode and 2-mode systems, respectively. Numerical experiments show that in each case the side-band growth is a function of $\mu/J$. For example, in the 1-mode system with $\varepsilon$ fixed, the evolution of $a_+(n)$ for $\mu = 22$, $J = 288$ matches that for $\mu = 11$, $J = 144$. Analogous properties hold for the 2-mode case. Experiments also show that side-bands do not grow if there is insufficient energy in the fundamental modes. For example, no growth was observed in the 1-mode system with $E = 0.02$.

Figures 5a–c show the solution profile for the 1-mode system at $n = 100$, 145, 155 with $E = 0.2$, $J = 120$, $\mu = 3$ and $\varepsilon = 0.000005$. Numerical results reveal that mode numbers 3, 37, and 43 are immediately stimulated, as suggested by the analysis in Section 4. The initial value of $|a_+(n)|$ is $\sqrt{2}\,\varepsilon$, and the maximum value of $|a_+(n)|$ has increased to 0.084 at $n = 155$. The graphs show the development of the instability as the side-bands grow. There is a local focusing of the instability and little evidence of the anticipated periodicity with wavelength $1/\mu = \frac{1}{3}$ in the modulated envelope. The growth rate of $a_-(n)$, $a_+(n)$ and $b(n)$ (see (4.1)) was found to vary with $\mu$, with an increase in growth rate as $\mu$ increases from zero. The more rapid growth rate at $\mu = 10$ is shown in Figs. 6a–c where the solution is given for $n = 70$, 90, and 92. This solution became unbounded before $n$ reached 100.

A random number generator was used to stimulate all Fourier modes with noise of controllable amplitude. Stimulation of this type is provided by roundoff at an amplitude determined by machine accuracy. With $J = 120$, $E = 0.2$ and noise of

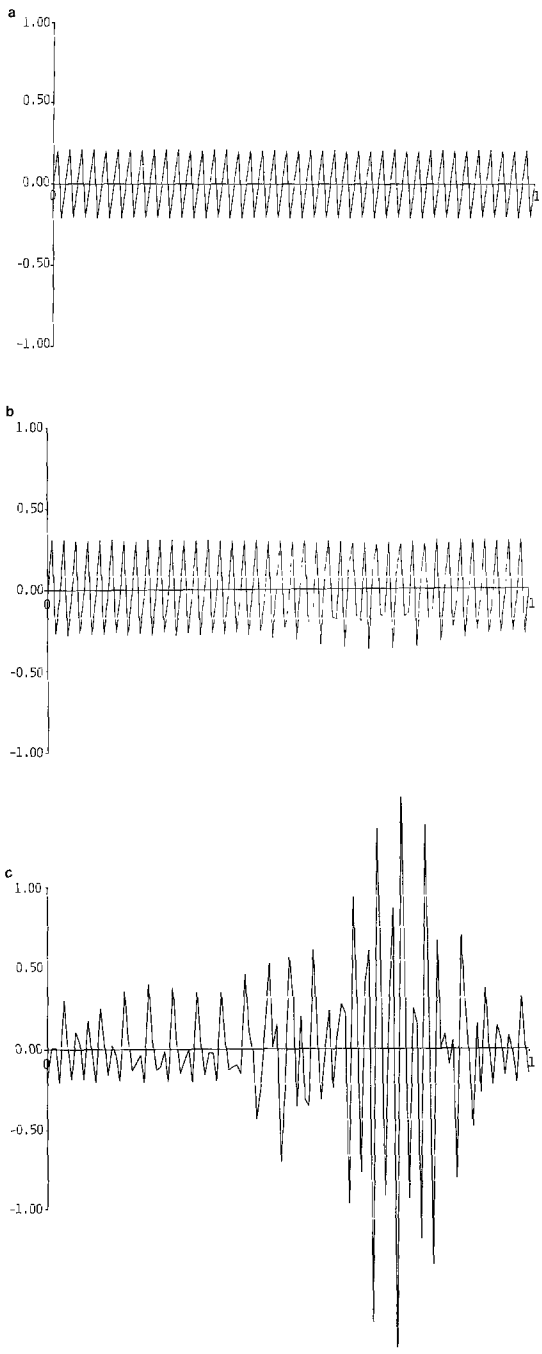


FIG. 5. Solution of 1-mode system with $E=0.2$, $J=120$, $\mu=3$ and $\varepsilon=0.5(-5)$. (a)–(c) Profiles at $n=100$, 145, 155.

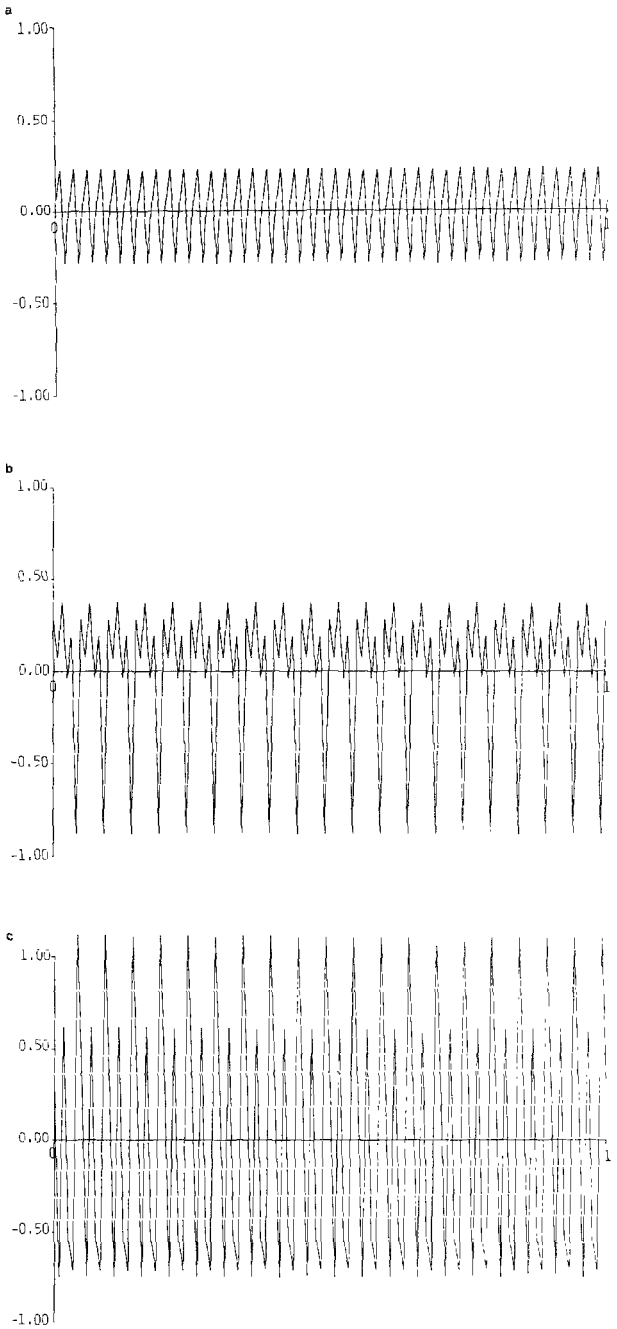


FIG. 6. Solution of 1-mode system with $E = 0.2$, $J = 120$, $\mu = 10$ and $\varepsilon = 0.5(-5)$. (a)–(c) Profiles at $n = 70$, 90, 92.

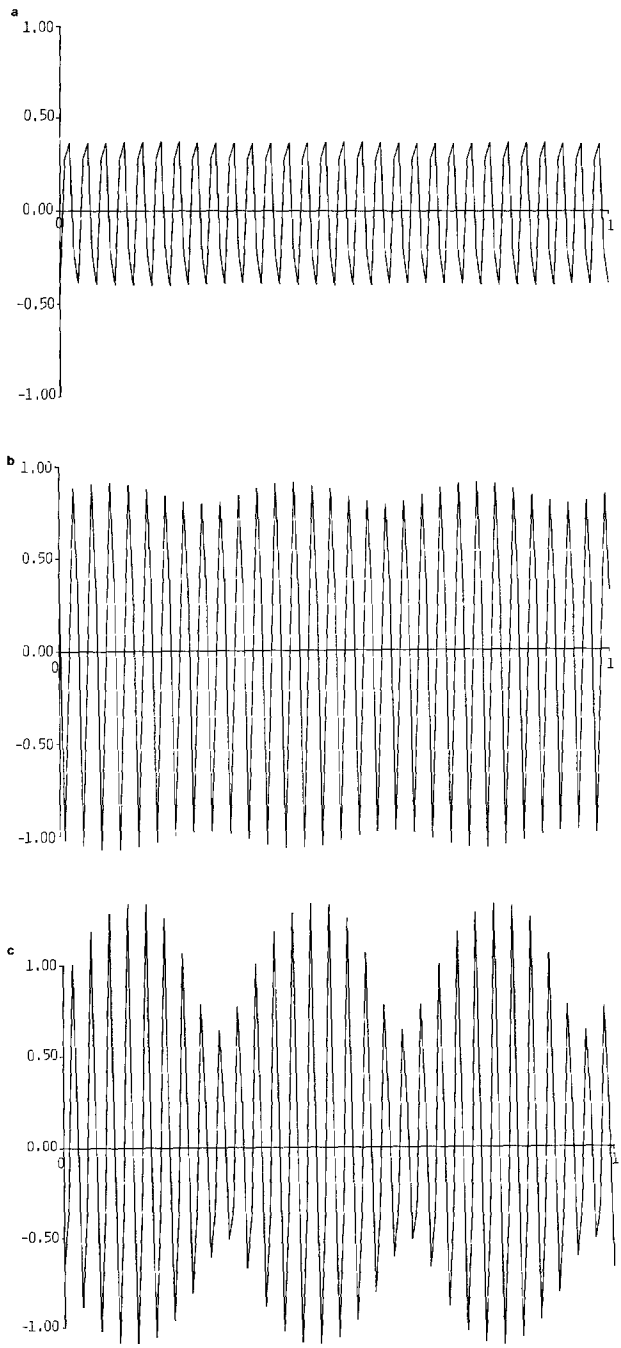


FIG. 7. Solution of 2-mode system with $E = 0.4$, $J = 120$, $\mu = 3$ and $\varepsilon = 0.5(-5)$. (a)–(c) Profiles at $n = 30$, 55, 70.

maximum amplitude $0.5(-8)$ the greatest growth rate was observed in mode numbers 20 and 60. This observation agrees with the observations made in Section 4 on the solution of (4.3) by the midpoint rule. There was no evidence of large growth rates in modes close to the fundamental.

Figures 7a–c show the solution for the 2-mode system at $n = 30$, 55, 70, with $E = 0.4$, $J = 120$, $\mu = 3$ and $\varepsilon = 0.000005$. In this case mode numbers 3, 27, 33, and 57 are immediately stimulated and their growth rates and magnitudes are comparable as $n$ increases. Note the distinct modulation with wave length $1/\mu = \frac{1}{3}$ in the 2-mode case. The maximum growth rate appeared to be around $\mu = 10$ when $J = 120$ and $E = 0.4$. Figures 8a, b show the solution corresponding to $\mu = 10$ for $n = 30$ and $n = 55$. This solution became unbounded before $n$ reached 70. In this case the use of a random number generator produced clear evidence of maximum growth rates in side-bands like those in (4.13), with $\mu/J$ approximately equal to 0.1.

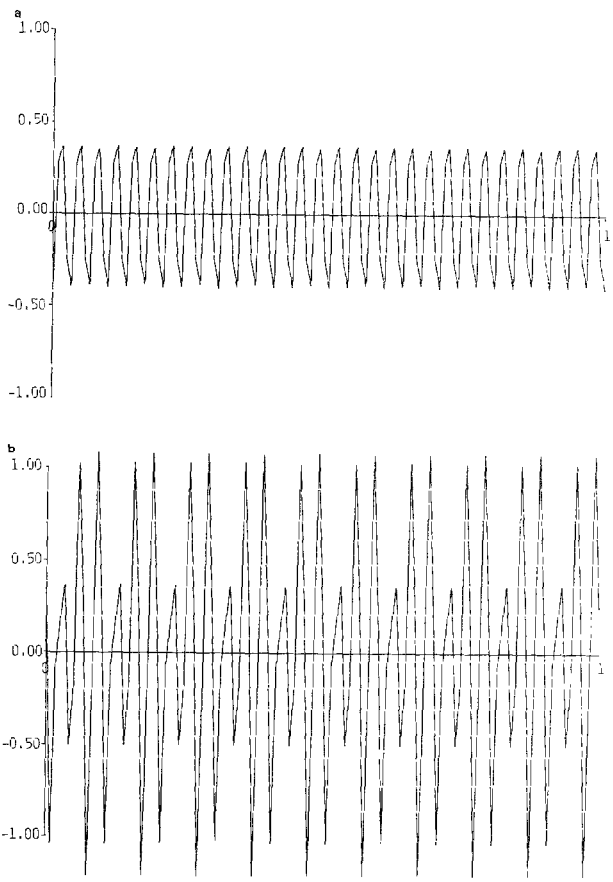


FIG. 8. Solution of 2-mode system with $E = 0.4$, $J = 120$, $\mu = 10$ and $\varepsilon = 0.5(-5)$. (a), (b) Profiles at $n = 30$, 55.

This gives good agreement with the aforementioned observations, but it differs from the observaions made by Briggs *et al.* [3] on the 2-mode system. With $J = 300$ they found maximum growth rate in mode numbers 72 and 78 which corresponds to $\mu/J = 0.01$. They used $E = 0.15$ and at this value of $E$ we observed no side-band growth over 2000 time steps.

## 6. Comments

The analysis and numerical experiments show the relation between leap-frog instabilities and Fourier side-band growth. The agreement between analysis and experiment is more obvious in the 2-mode system. Variation of growth with $\mu$ has been demonstrated and reference is made to the existence of a maximum growth rate at some $\mu > 0$. Figure 7 shows the anticipated relation between side-band growth and envelope modulation. Analysis and experiment show that side-band growth is absent if there is insufficient energy in the fundamental modes. The analysis suggests that the growth is related to the midpoint rule time discretisation. To check this the semi-discrete system (2.8) was written as $d\mathbf{U}/dt = \mathscr{L}(\mathbf{U})$ and integrated usng the implicit method

$$\mathbf{U}^{n+1} - \mathbf{U}^n = k\mathscr{L}(\tfrac{1}{2}(\mathbf{U}^n + \mathbf{U}^{n+1})). \tag{6.1}$$

If $\theta = \frac{2}{3}$ method (6.1) satisfies the conservation condition

$$\sum_{j=0}^{J-1} (U_j^{n+1})^2 = \sum_{j=0}^{J-1} (U_j^n)^2.$$

The 2-mode system with $E = 0.4$, $J = 120$, $\mu = 3$ and $\varepsilon = 0.000005$ was integrated over 200 steps using (6.1). Throughout the integration there was no growth in mode numbers 3, 27, 33, and 57. Briggs *et al.* [3] have made several suggestions concerning the prevention of nonlinear instabilities of the type described in this paper.

The work described here adds to the interesting ideas proposed by Newell [8] and developed by Briggs, Newell and Sarie [3] on a mechanism which may lead to destabilisation of "stable" difference solutions. The stable solutions considered consist of isolated Fourier modes which are regarded as perturbations about a non-zero, constant solution. The destabilisation process involves an accumulation of energy by additional Fourier modes in situations where the overall energy is not conserved. The work described in Section 5 shows that growing Fourier modes may be stimulated using a random number generator, and this suggests that in a real calculation over a long period of time the stimulation may be effected by roundoff errors. The question which still has to be answered, of course, is whether roundoff errors will stimulate growing Fourier modes when the basic solutions are more general than those considered here. The answer to this question will only come from more analysis and more numerical experimentation. If instabilities of the type considered arise in practical calculations using leap-frog methods, then effective

methods of suppressing the instabilities should be constructed. This will require a better understanding of the mechanisms involved.

## ACKNOWLEDGMENT

The authors are grateful to Professor John Hunter, Department of Mathematics, Colorado State University, for suggesting the inclusion of material on multiple time scales to indicate possible limitations in the model described by (4.7).

## REFERENCES

1. T. B. BENJAMIN, *Proc. R. Soc. London A* **299**, 59 (1967).
2. T. B. BENJAMIN AND J. E. FEIR, *J. Fluid Mech.* **27**, 417 (1967).
3. W. L. BRIGGS, A. C. NEWELL, AND T. SARIE, *J. Comput. Phys.* **51**, 83 (1983).
4. B. FORNBERG, *Math. Comp.* **27**, 45 (1973).
5. B. FORNBERG AND G. B. WHITHAM, *Philos. Trans. R. Soc. London* **289**, 373 (1978).
6. B. M. HERBST, A. R. MITCHELL, AND J. A. C. WEIDEMAN, *J. Comput. Phys.* **60**, 263 (1985).
7. M. J. LIGHTHILL, *J. Inst. Math. Appl.* **1**, 269 (1965).
8. A. C. NEWELL, *SIAM J. Appl. Math.* **33**, 133 (1977).
9. L. N. TREFETHEN, "Nonlinear Instability of Difference Models of $u_t = -uu_x$," MIT, 1983 (unpublished).
10. F. VADILLO AND J. M. SANZ-SERNA, Submitted for publication.
11. G. B. WHITHAM, *Linear and Nonlinear Waves* (Wiley, New York, 1974).
12. H. C. YUEN AND W. E. FERGUSON, *Phys. Fluids* **21**, 1275 (1978).